NONLINEAR DYNAMIC ANALYSIS OF A SATELLITE COMPONENT MODELED AS A MULTI-MASS SYSTEM

Lucas Sardinha de Arruda

arrudalucas@usp.br

Universidade de São Paulo
Av. Prof. Almeida Prado, trav.2 nº. 83 Cidade Universitária, 05508-900, São Paulo, São Paulo, Brazil

Reyolando M.L.R.F. Brasil

reyolando.brasil@ufabc.edu.br

Universidade Federal do ABC, São Bernardo, Brazil.
Alameda da Universidade, s/n, Bairro Anchieta, 09606-045, São Bernardo do Campo, São Paulo, Brazil

Abstract. *Over the last decades, the Brazilian Space Agency (AEB) has received a small, but significant investment in its space program, focusing on the establishment and development of its communication network. This improvement, led by the CBERS project (China-Brazil Earth-Resources Satellite) and the launch of the Geostationary Defense and Strategic Communications Satellite (SGDC system), has created a landmark in the national space program, giving a new perspective for R&D in the area. In this context, we intended to perform a set of tests aiming at the creation of software to simulate the dynamic behavior of lightweight and flexible structures in orbit. The dynamic analysis of these flexible components (such as, solar sails or antennas) will be carried out by systematic time numerical integration based on the Newmark's method and implemented on MatLab® language; with the dynamic balance of at each time step obtained through Newton-Raphson's method. Finally, a multi-mass structure has been develop for a comparative study between the dynamic response of linear and nonlinear models, showing the importance of a nonlinear approach in the design of a lightweight and flexible structures.*

Keywords: *Newmark-beta method, Newton-Raphson's method, Nonlinear Dynamic Analysis, Multi-mass System, Satellite Component.*

INTRODUCTION

Technological advances in the development of high-performance composite materials concurrently with new manufacturing techniques (such as, miniaturization of components and subsystems) and next-generation design of deployment mechanisms has allowed uprising of spacecraft state-of-art technologies, mainly focused on small satellite – e.g. CubeSat (an U-class Spacecraft). These technological developments have contributed to the steadily increase in R&D investment - on account of its affordable deployment cost, better performance, cost-effectiveness and reliable design. It has expanded its application range to areas formerly achievable only by large-scale satellites, such as, broadcasting, communication, meteorology. Its vast potential for space-based internet services and real-time satellite scanning has renewed the Brazilian market investments in small satellites, leading to the creation of partnership programs such as the CBERS project (China-Brazil Earth-Resources Satellite) and the launch of the new Geostationary Defense and Strategic Communications Satellite (SGDC system).

It is worth mentioning that the technological advances in spacecraft appendages and hardware were only achieved through simultaneously development in structural booms and arrays technologies, since some components require large structures for energy harvesting (e.g. Solar Sail) or to support a single tip mass in order to limit the influence of the inherent satellite magnetic field. Therefore, the current engineering challenge, and main goal of this work, is to quantify and predict the structural behaviors, especially with respect to lightweight and flexible structures. In this context, we perform a literature review about lightweight and flexible structures, focusing on the development of a multi-mass structure for a comparative study between the dynamic response of linear and nonlinear models.

Belvin, et al. (2016) provides a state of the art overview on deployable booms and existing spacecraft deployable appendages. In addition, the author discuss about the challenge and limitations of a reliable and efficient boom deployment, thus justifying the recent studies and advances in the area. Similarly, Fetchko, et al. (2004) describes the deficiencies in current flight-heritage booms, arguing that the technological advances in spacecraft appendages, such as the micro-propulsion ion thrusters, are limited by the old-fashion structural boom designs. Moreover, Fetchko, et al. (2004) highlights the development of Elastic Memory Composite (EMC) materials, showing its advantages over other materials.

Tupper, et al. (2001) propose a hierarchical multidisciplinary approach to explain how the Elastic Memory Composite (EMC) materials enable a composite structure or component to be deformed/folded for efficient packaging, without any apparent degradation of his material properties, eliminating the shortfalls of current composite deployable spacecraft structures. Straubel, et al. (2011) introduces the concept of the Carbon fiber reinforced polymers (CFRP) booms, comparing their performance with other structural models, such as pantographic structures, inflatable structures and elastically deformable systems. Additionally, the author conducts tests under artificial zero-g environment to verify the applicability of these concepts, justifying future works in the area.

1 FalconSAT-3 Boom: A Multi-Mass System Approach.

In this work, we use a multi-mass model based on the FalconSAT-3 boom to develop a reliable software that can quantify and predict the structural behavior of light structures in orbit, as well as perform a nonlinear dynamic study of structural booms designs, see Fig. 1. The FalconSAT-3 program was chosen as the primary example of this work because its main objective -a study of innovative, highly efficient boom deployment technologies - is the topic of several works in the specialized literature; see Fetchko, et al. (2004) and Liu, et al. (2014).

The U.S. Air Force Academy FalconSAT program consists of a partnership between the U.S. Air Force Academy (USAFA) and outside organizations – such as the Air Force Research Laboratory (AFRL) - focusing on the development of small satellites to conduct Department of Defense space missions. This program gives the academy cadets an opportunity to carry out the design, analysis, construction, testing and operation of these satellites.

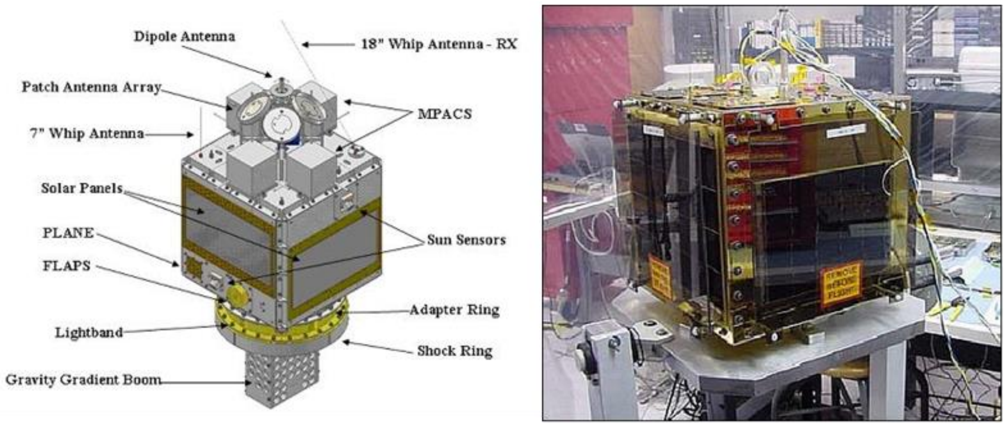

Figure 1. View of the FalconSat-3 (Image credit: USAFA).

The FalconSat-3 satellite is a small scale, low-cost project - similar to previously FalconSAT missions - that has as main objectives: (1) a feasibility test of a highly efficient boom deployment technology based on EMC material, and (2) the study of the space environment, accomplished through several sponsored experiments. Some of these experiments being carried out in collaboration with the Academy Physics Department, as the FLAPS (Flat Plasma Spectrometer). In the other hand, there is the Micro Propulsion Attitude Control System (MPACS) being developed in partnership with the Air Force Research Lab's Propulsion Directorate (AFRL).

Figure 1 presents a full view of the FalconSat-3 satellite, showing its spacecraft appendages and experiments, similarly, Table 1 gives us the satellite and boom dimensions in its deployed configuration. This information is used in the development of our computational model.

Table 1. FalconSat-3 dimensions in a deployed configuration (Fetchko (2004)).

Properties	Value
Total Mass [kg]	$5.43 \text{x} 10^{01}$
Total Boom Mass [kg]	$9.00 \text{x} 10^{00}$
Tip Mass [kg]	$7.80 \text{x} 10^{00}$
Boom Length [m]	$3.38 \text{x} 10^{00}$
Satellite Dimensions [m] (see Fig.2)	$4.33 \text{x} 10^{-01}$
	$7.87 \text{x} 10^{-01}$
	$4.33 \text{x} 10^{-01}$
Tip Dimensions [m] (see Fig.2)	$2.79 \text{x} 10^{-01}$
	$3.99 \text{x} 10^{-01}$
Moment of Inertia -Annulus [m^4]	$4.11 \text{x} 10^{-09}$

As described before, the main objective of the FalconSat-3 satellite is testing new designs, materials and deployment techniques in structural booms and arrays. Nonetheless, the program also studies its application as a tool for passive gravity gradient stabilization of the spacecraft. For this reason, the FalconSAT cadets seek the development/use of a new composite material – the TEMBO® EMC, a high performance composite with a polymer resin that exhibits shape memory properties – capable to support the packing/deploy cycle required by the mission. Following the approach developed by Fetchko, et al. (2004), we assume that the structural properties of the TEMBO® EMC material are derived from the S2-Glass / Epoxy composite – the composite properties being shown in the Table 2 (extract from Military Handbook - Composites (2002)).

Table 2. S2-Glass/Epoxy Composite (ref. Military Handbook - Composites (2002)).

S2-449 43.5k/SP 381 Unidirectional Tape	
Fiber Properties	Value
Fiber Density [kg/m^3]	$2.490 \text{x} 10^{+03}$
Resin Density [kg/m^3]	$1.216 \text{x} 10^{+03}$
Composite Density [kg/m^3]	$1.850 \text{x} 10^{+03}$
Fiber Areal Weight [kg/m^2]	$2.840 \text{x} 10^{-01}$
Fiber Volume [%]	$5.000 \text{x} 10^{+01}$
Ply Thickness [m]	$2.290 \text{x} 10^{-04}$
Transverse Elastic Modulus [N/m^2]	$4.760 \text{x} 10^{+10}$

Lastly, we opted to simulate the loading applied the structure as a satellite attitude control situation, performed in two different loading cases: (a) the first phase consists in the application of a 'hypothetical' harmonic load to the tip of the boom, its frequency close to the first natural frequency of the structure; (b) in the second phase, we apply a harmonic load, whose magnitude decays with time according to an exponential function - simulating a satellite control situation. Furthermore, it was decided to discard the amplitude force value given by the MPACS, due to its magnitude-time relation, choosing instead an amplitude force range (F_0) between a typical small/medium scale satellites (as described in Dankanich (2015) – Green Liquid Propulsion), and a 'hypothetical' maximum value of $500N$.

1.1 Multi-Mass Model.

In this work, a multi-mass model is proposed, as shown in Fig.2, to describe the dynamic behavior of the FalconSat-3 boom. The develop model was chosen because of its simplicity. The equations of motion, as well as their computational implementation can be easily deduced and adapted for several problems. Nevertheless, the model provides a dynamic response close to expected, taking into account the limitations of the adopted model.

Initially, we assume a multi-mass model consisting of n elements, each one formed by a lumped mass m_i, located at its upper end and connected to each other by an inextensible spring modelled as an inextensible Euler beam with equivalent stiffness k_i, only acting on the transverse displacement. In this initial stage, it is assumed that the structural boom has a uniform mass distribution, thus allowing each element to have a mass given by $\mathrm{m_i} = M/n$, leading to the simplification of the global mass matrix (M).

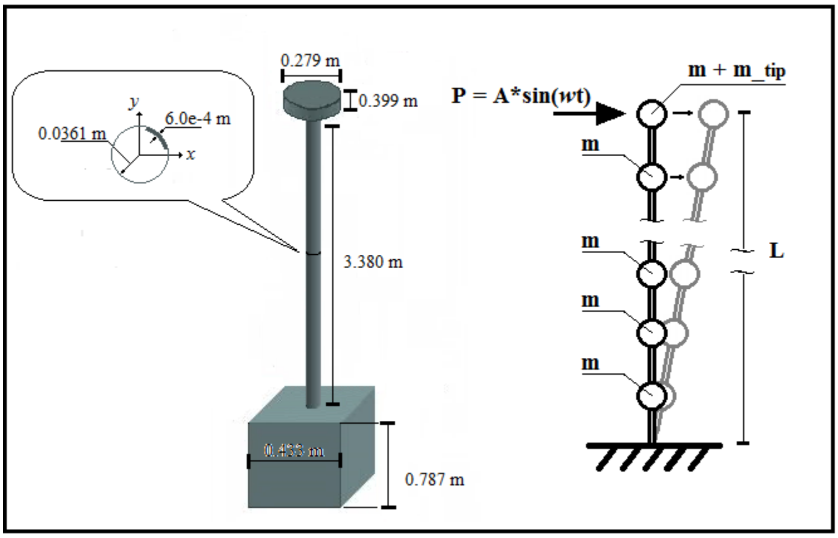

Figure 2. FalconSat-3 deployed dimensions (Left - Image credit: USAFA) and the multi-mass model used to describe the structural boom (Right).

In addition, we assume that the stiffness related to the transverse displacement of each element is much larger than the stiffness related to the rotation, and ignore the damping effects of the global structure. Therefore, we have:

$$k_i = 12EI/l^3 \tag{1}$$

where E is the elastic modulus of the material, in this case, the S2-Glass/Epoxy composite, I is the cross-sectional inertia moment of the boom, assumed constant throughout the structure, and l the size of each element, given by $l = L/n$. It is worth mentioning that this specific modeling has a peculiar characteristic: any change in the number of elements (n) affects the structure flexibility, and consequently, its natural frequency.

Based on the hypotheses previously described, and assuming a multi-mass model of n elements, as shown in Fig.2, we have that for a generic i-element, the balance of forces is given by:

$$m_{\mathrm{i}}\ddot{u}_{\mathrm{i}} + k_{\mathrm{i}}(u_{\mathrm{i}} - u_{\mathrm{i}-1}) - k_{\mathrm{i}+1}(u_{\mathrm{i}+1} - u_{\mathrm{i}}) = f_{\mathrm{i}}(t) \tag{2}$$

where m_i is the lumped mass for the i-element ($m_i = M/n$), k_i is the equivalent spring stiffness, usually modelled as an Euler beam element, as previously described, and $F_i(t)$ represents the load term which the i-element is subjected. From Eq. (2), It is possible to observe that for a n-element model, the inertial forces terms are constants (Eq. (3)).

$$F_{I_i} = m_i\ddot{u}_i \tag{3}$$

Simultaneously, the restorative terms are given by,

$$F_{R_i} = -k_i x_{i-1} + (k_i + k_{i+1})x_i - k_{i+1}x_{i+1} \tag{4}$$

It should be emphasized that the first and last elements have slightly different terms, described, respectively, by:

$$F_{R_1} = (k_1 + k_2)x_1 - k_2 x_2 \tag{5}$$

$$F_{R_n} = -k_n x_{n-1} + k_n x_n \tag{6}$$

Once we know the behavior of the linear model, it is possible to perform a simplified nonlinear analysis. For this, we assume that the nonlinear term is described as a third order polynomial ($b_i\Delta x^3$), acting on the model restorative forces. This adjustment, shown in Eq. (4), tries to approximate the dynamic response to the actual behavior of the structure. Therefore, we can rewrite the Eq. (2) as a sum of the linear and nonlinear terms, obtaining:

$$m_{\mathrm{i}}\ddot{u}_{\mathrm{i}} + [k_{\mathrm{i}}(u_{\mathrm{i}} - u_{\mathrm{i}-1}) + \mathrm{b}_{\mathrm{i}}(u_{\mathrm{i}} - u_{\mathrm{i}-1})^3] - [k_{\mathrm{i}+1}(u_{\mathrm{i}+1} - u_{\mathrm{i}}) + \mathrm{b}_{\mathrm{i}}(u_{\mathrm{i}+1} - u_{\mathrm{i}})^3] = f_{\mathrm{i}}(t) \tag{7}$$

Analogously to the linear case, we can perform a separation process of the restorative and inertial components for each element, obtaining the following relationship:

Proceedings of the XXXVIII Iberian Latin-American Congress on Computational Methods in Engineering
P.O. Faria, R.H. Lopez, L.F.F. Miguel, W.J.S. Gomes, M. Noronha (Editores), ABMEC, Florianópolis, SC, Brazil, November 5-8, 2017.

$$F_{I_i} = m_{\mathrm{i}}\ddot{u}_{\mathrm{i}} \tag{8}$$

and,

$$F_{R_i} = \left[-k_i x_{i-1} + (k_i + k_{i+1})x_i - k_{i+1}x_{i+1}\right] + [-b_i x_{i-1}^3 + \cdots$$
$$+ (b_i + b_{i+1})x_i^3 - b_{i+1}x_{i+1}^3 + 3b_i\left(x_i x_{i-1}^2 - x_i^2 x_{i-1}\right) - 3b_{i+1}\left(x_{i+1}x_i^2 - x_{i+1}^2 x_i\right)] \tag{9}$$

where k_i and b_i are the linear and nonlinear stiffness components of each element, respectively, and x_i describes the i-element displacement. Moreover, as a requisite of the Newton-Raphson's method, we need to specify the tangent stiffness matrix (or Jacobian matrix) component of each element, given by:

a. Linear case.

$$dR_{i,i-1} = -k_i \tag{10}$$

$$dR_{i,i} = k_i + k_{i+1} \tag{11}$$

$$dR_{i,i+1} = -k_{i+1} \tag{12}$$

b. Nonlinear case.

$$dR_{i,i-1} = -k_i - 3b_i x_{i-1}^2 + 3b_i\left(2x_i x_{i-1} - x_i^2\right) \tag{13}$$

$$dR_{i,i} = k_i + k_{i+1} + 3(b_i + b_{i+1})\,x_i^2 + 3b_i\left(x_{i-1}^2 - 2x_i x_{i-1}\right) + \cdots$$
$$-3b_{i+1}\left(2x_{i+1}x_i - x_{i+1}^2\right) \tag{14}$$

$$dR_{i,i+1} = -k_{i+1} - 3b_{i+1}x_{i+1}^2 - 3b_{i+1}\left(x_i^2 - 2x_{i+1}x_i\right) \tag{15}$$

Again, because the first and last elements have slightly different terms, a change in Eq. (10)-(15) will be required. Finally, we can write the set of partial differential equations that govern the problem as,

$$F_I + F_D + F_R = f(t) \tag{16}$$

In the absence of dissipative forces, Eq. (16) becomes,

$$F_I + F_R = f(t) \tag{17}$$

where the inertial and restorative terms are given by Eqs. (3)-(4), for a linear case; and Eqs. (8)-(9), otherwise.

1.2 Newmark's Method.

Once we known the partial differential motion equations that govern the problem, Eq. (17), it is possible to use a numerical methodology, such as the Newmark's method, as a way of study the dynamic behavior of the modeled structure, considering that, in most cases, obtaining the analytical solution for the model can become an intractable problem.

The main idea behind the Newmark's method is the development of a prediction step, where the generalized variables at a final time t_f – endpoint of the interval dt - are based on the values at the initial time t_i; thus solving the motion equations in an incremental way. Based on this premise, we use the generic dynamic equilibrium equation, presented in Eq. (18), as a starting point to develop the method throughout this section:

$$F_I + F_D + F_R = f(t) \tag{18}$$

where F_I, F_D and F_R are the inertial, dissipative and restorative force component, respectively, and $f(t)$ represents the generalized load applied to the system, which may or may not be function of time, acceleration, displacement and/or velocity. The relation between the generalized variables at the two endpoints of a generic interval is given by following equations:

$$\delta u = u^{t_f} - u^{t_i} \tag{19}$$

$$\dot{u}^{t_f} = b_0 \delta u - b_2 \dot{u}^{t_i} - b_3 \ddot{u}^{t_i} \tag{20}$$

$$\ddot{u}^{t_f} = b_1 \delta u - b_4 \dot{u}^{t_i} - b_5 \ddot{u}^{t_i} \tag{21}$$

where the coefficients b_k (k = $0, 1, \dots, 5$) - chosen by the user beforehand - are related to the method's precision and stability. Assuming the premise of constant average acceleration between the two endpoints (t_f & t_i), we assign the following values to the constants b_k ,

$$b_0 = 4/(\delta t^2), \quad b_1 = \, 2/(\delta t), \quad b_2 = \, 4/(\delta t), \quad b_3 = 1, \quad b_4 = 1, \quad b_5 = 0 \tag{22}$$

It is noteworthy that a constant average acceleration assumption between the two interval endpoints leads to an unconditionally stable method for the resolution of linear problems. Rewriting the generic dynamic equilibrium, Eq. 18, as a residual function, we obtain

$$\mathrm{g}(u, \dot{u}, \ddot{u}) = f(t) \tag{23}$$

For the next time step, Eq. (24), we write the force residue $\hat{f}$ at time t_f as an approximation of u^{tf}, obtained from a previous iteration.

$$ {}^{j}\hat{f}^{tf} = f^{ti} - h\left({}^{j}u^{tf} \right) \tag{24}$$

where $h\left({}^{j}u^{tf} \right)$ is an explicit function of the displacements at the time t_f, obtained from Eq. (23) by the introduction of the prediction step relations. For the next iteration, we look for a new approximation ${}^{j+1}u^{tf}$, such that ${}^{j+1}\hat{f}^{tf} \approx 0$. Expanding the residue function in the neighborhoods of ${}^{j}u^{tf}$ in Taylor series, we have

$$ {}^{j+1}\hat{f}^{tf} = {}^{j}\hat{f}^{tf} + {}^{j}\left[\partial\hat{f}/\partial u\right]^{tf\, j+1}\delta u + \cdots = 0 \tag{25}$$

Finally, disregarding the higher order terms, we arrive at the relation:

$$ - {}^{j}\left[\partial\hat{f}/\partial u\right]^{tf\, j+1}\delta u = {}^{j}f^{tf} \tag{26}$$

where the term $- {}^{j}\left[\partial\hat{f}/\partial u\right]^{tf}$ is the gradient matrix of the process, where the equilibrium iterations (Eq. (26)) are solved by an iterative method, such as the Newton-Raphson method.

Wriggers (2008) presents the mathematical formulation of the method, as well as, the Newton-Raphson iterative process and several linear/nonlinear examples. A directly approach of the method is presented in Brazil (1990), were we can find some non-linear application, along with a Fortran© implementation.

1.3 Results.

Based on the Multi-mass model described in Section 1.2, we intend to perform a set of tests, to compare the dynamic behavior of the linear and nonlinear model under the influence of a harmonic load. For this reason, a 20-element multi-mass structure is used to model the FalconSat-3 boom. In order to obtain the values of the lumped mass (m_0), the equivalent spring stiffness (k_0) and consequently the first natural frequency (ω_1) of this system, we use the boom dimensions and properties presented in Table 3.

From the data presented in Table 3, it is possible to determine the equivalent stiffness (assumed constant for all elements) given by $k_0 = 5.2237\text{x}10^5$ Nm. Similarly, the lumped mass of each element is given by $m_0 = 0.45$ kg. One should note that the tip mass must be increased by the Thruster mass (Tip mass). After the global matrices building phase, it is possible to determine the vibration modes - as well as the respective natural frequencies of the structure - by solving the eigenvalue problem, where the first natural frequency is given $\omega_1 = 48.2859$ rad/s.

Table 3. Structural properties used to design the multi-mass model.

Properties	Nomenclature	Value
Total Boom Mass [kg]	M	$9.00\text{x}10^{00}$
Tip Mass [kg]	M_{tip}	$7.80\text{x}10^{00}$
Boom Length [m]	L	$3.38\text{x}10^{00}$
Elastic Modulus $[\text{N}/\text{m}^2]$	E	$4.76\text{x}10^{+10}$
Moment of Inertia - Annulus $[\text{m}^4]$	I	$4.11\text{x}10^{-09}$

The nonlinear parameter b_0 was chosen to obtain a polynomial stiffness function that has the best fit to a resonable 'force-displacement' curve, as shown in Fig.3, where the term $b_0 = -20\text{k}_0$ refers to the cubic term of a polynomial function. This parameter is based on the hypothesis that after a certain displacement x_{limit} the model stops behaving linearly and assumes a parabolic profile. Additionally, we set the control parameters of the simulation, using a minute timestep ($\Delta\text{t} = 10^{-4}$ s) for a simulation time of ten seconds ($\text{t}_{\text{final}} = 10$ s).

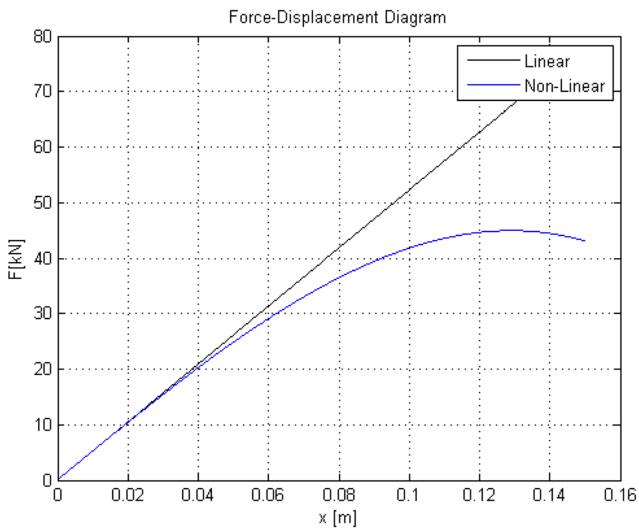

Figure 3. Comparative curves for the linear and nonlinear stiffness - Beam element.

From the application of a harmonic load ($f_n(t) = F_0\sin(\omega\text{t}) = 10^2\sin(0.80\omega_1)$, where F_0 is the load magnitude and ω_1 the first natural frequency) to the upper element of the linear model, simulating a thruster control condition, we obtain the displacement curves shown in Figure 4. From Fig.4, it is possible to observe the occurrence of displacement peaks at intervals of 0.15 s, approximately - indicating a frequency of 7.68 Hz; the upper element being responsible for the maximum displacement - approximately 0.018 m.

Proceedings of the XXXVIII Iberian Latin-American Congress on Computational Methods in Engineering
P.O. Faria, R.H. Lopez, L.F.F. Miguel, W.J.S. Gomes, M. Noronha (Editores), ABMEC, Florianópolis, SC, Brazil, November 5-8, 2017.

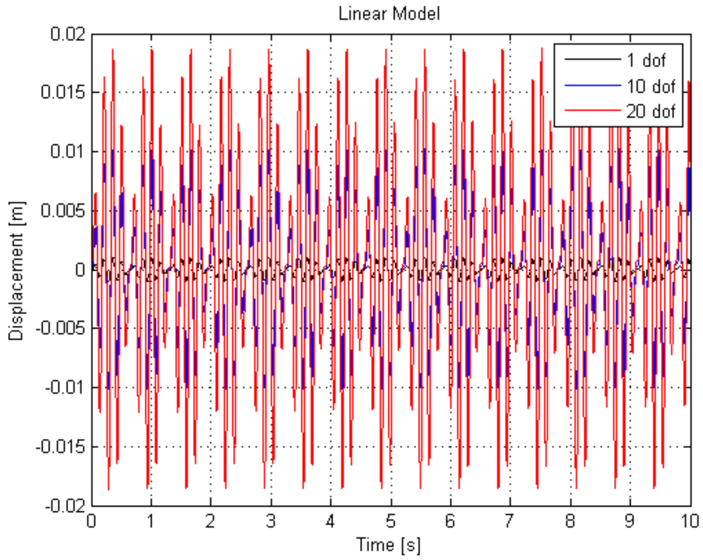

Figure 4. Time history of Multi-mass displacement for a harmonic load with frequency $\boldsymbol{\omega = 0.80\omega_1}$.

Following the same procedure performed for the linear model, Fig. 4, we obtain the displacement behaviour for the nonlinear model under the influence of a harmonic load $f_n(t) = F_o \sin(\omega t)$ applied at the tip element, thus allowing us to overlap the upper element displacement curves for both models, see Fig.5, to study their correlation.

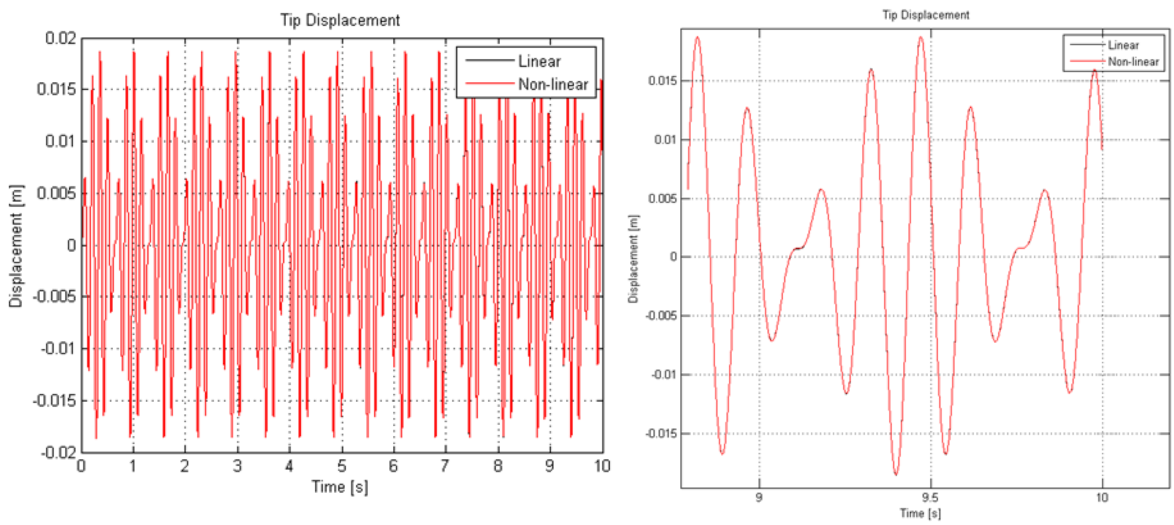

Figure 5. Time history of Multi-mass displacement for a harmonic load with frequency $\boldsymbol{\omega = 0.80\omega_1}$ – Comparative analysis between linear & nonlinear models (Zoom - left).

Analyzing the dynamic response of both models to a harmonic load $f_n(t) = 10^2 \sin(0.8\omega_1 t)$, see Fig.5, we notice a very small difference in the amplitude of both curves close to the time $\mathrm{t} = 9.15$ s. However, with the exception of this single event, we see that both models – linear and nonlinear – present an similar dynamic behavior, showing the exact displacement peaks, as well as values of extrema. From Fig.5, it is possible to observe that the displacement peak has a amplitude of 0.018m, corresponding to a linear region of the stiffness curve (Fig.3), where both models are described as the same function.

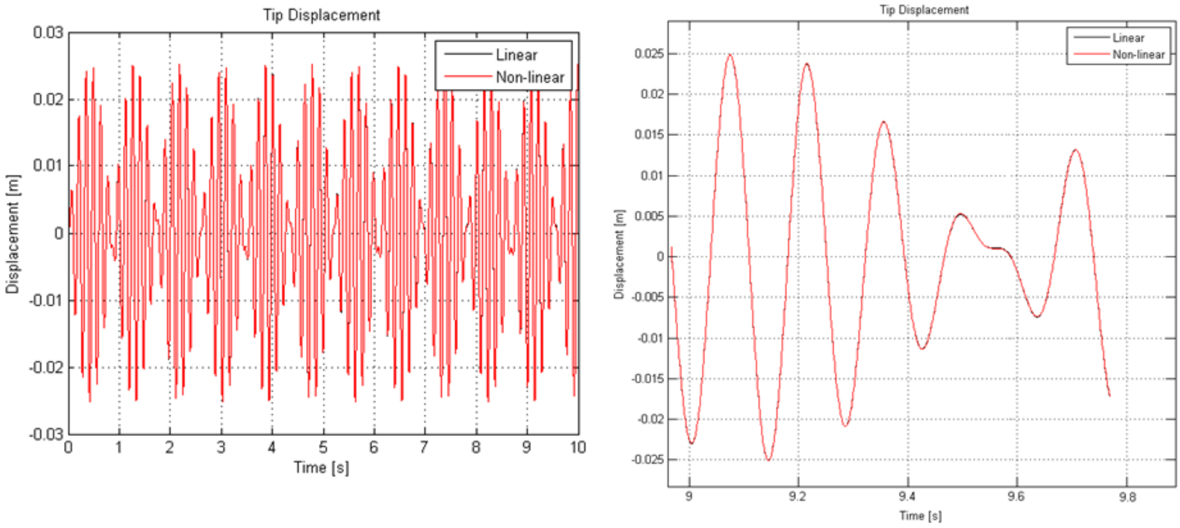

Figure 6. Time history of Multi-mass displacement for a harmonic load with frequency $\boldsymbol{\omega = 0.85\omega_1}$ – Comparative analysis between linear & nonlinear models (Zoom - left).

Assuming another harmonic loading condition, where the frequency is increased to a new value, given by $\omega = 0.85\omega_1$ (Fig.6); we can observe a slightly increase in the maximum displacement for both models - $d_{peak} = 0.025\ m$ – changing the point stiffness curve (Fig.3) to a new region, where the difference between these two models still negligible. An interesting data is found during the time interval between [9.5-9.6], where the displacement difference (Δd) between these two models becomes visible, but still very small – $\Delta d_{peak} = 10^{-5}$ m.

It should be noted that in this first part of the results, a series of simulations were developed, trying to study the effect of the applied load frequency on the linear and nonlinear dynamic behavior. For this reason, Fig. 7 presents the dynamic behaviour for a harmonic condition with a new frequency $\omega = 0.90\omega_1$.

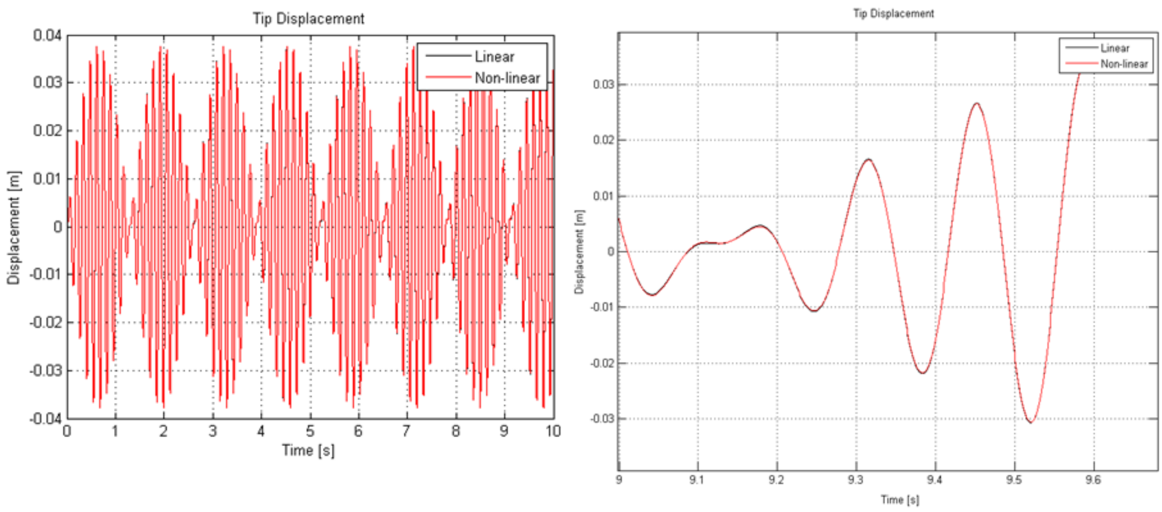

Figure 7. Time history of Multi-mass displacement for a harmonic load with frequency $\boldsymbol{\omega = 0.90\omega_1}$ – Comparative analysis between linear & nonlinear models (Zoom - left).

Based on Fig. 7, we have that the response curves still shows a displacement peaks within the linearity region ($d_{peak} = 0.03$ m, see Fig. 3), presenting a similar behavior, as observed in both images. Notwithstanding, we see a small increase in the comparison process, since the difference peak Δd_{peak} reaches the 10^{-4} m scale within the time interval of [9.1-9.2] s.

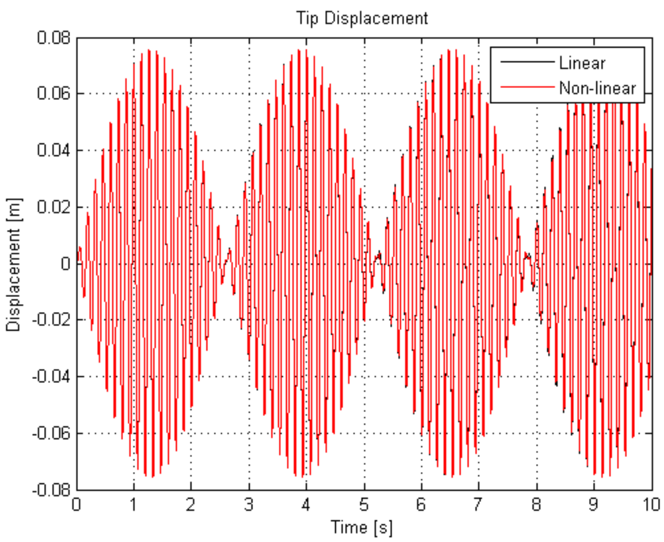

Figure 8. Time history of Multi-mass displacement for a harmonic load with frequency $\boldsymbol{\omega = 0.95\omega_1}$– Comparative analysis between linear & nonlinear models.

Next, we apply a harmonic load with a frequency value extremely close to the first natural frequency ($\omega = 0.95\omega_1$), where the displacement amplification leads the model to a nonlinear region in the stiffness curve ($d_{peak} = 0.06$ m, see Fig. 3). Figures 8 and 9 present the dynamic behavior of the FalconSat-3 boom near the resonance regime, where we can see an increase in the displacement peak, going from 0.03 m to 0.06 m. Moreover, it is possible to notice a difference between these two models near the time interval [7.4 – 8.0]s. This amplification is typical of structures close to the resonance regime, since a small increment in the load frequency is responsible for introducing more and more energy to the system, which in the absence of dissipative forces, may end up leading to a critical condition, resulting in failures and loss function.

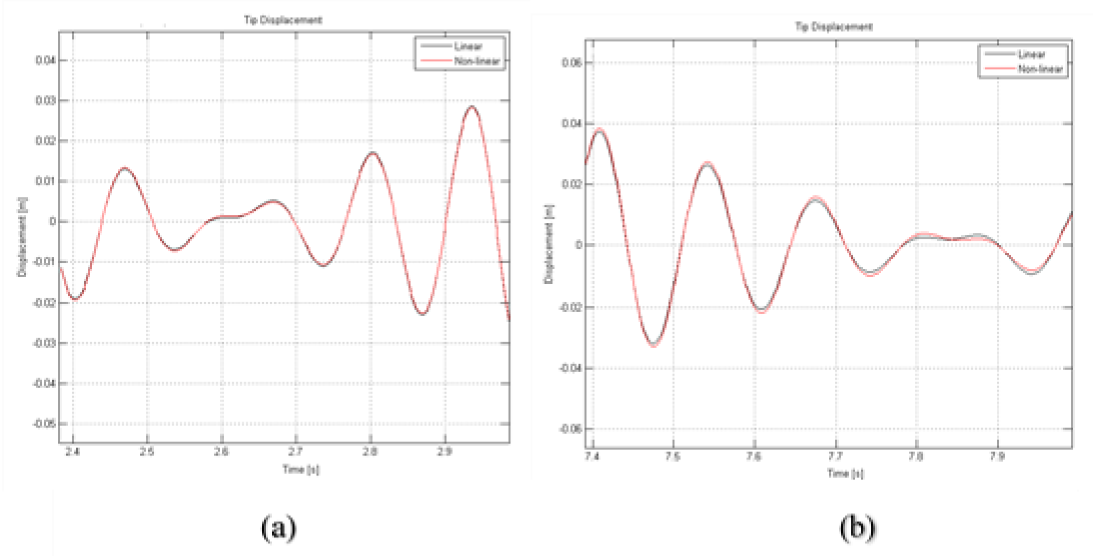

Figure 9. Time history of Multi-mass displacement for a harmonic load with frequency $\boldsymbol{\omega = 0.95\omega_1}$ – Comparative analysis between linear & nonlinear models (Zoom); where (a) and (b) represent different time intervals.

A similar analysis as the one performed for the frequency is carried out, where we try to study the effects of the amplitude on the linear and nonlinear dynamic behavior, simulating a design condition were high-power thrusters are used. Figure 10 presents the displacement curves for a load condition with $F_0 = 200$ N and frequency set to $\omega = 0.9\omega_1$.

For this load condition, where the maximum displacement (d_{peak}) is located near the inflexion point of the polynomial approximation (Fig.3), we can notice an unusual behavior of the nonlinear model, especially when we consider flexible structures under the influence of increasing loads, as shown in Fig.11. This difference is a result of the stiffness loss felt by each nonlinear element. Thus, we see an increment in the peak's gap, where Δd_{peak} reaches the 10^{-3} m scale in several time intervals.

Proceedings of the XXXVIII Iberian Latin-American Congress on Computational Methods in Engineering
P.O. Faria, R.H. Lopez, L.F.F. Miguel, W.J.S. Gomes, M. Noronha (Editores), ABMEC, Florianópolis, SC, Brazil, November 5-8, 2017.

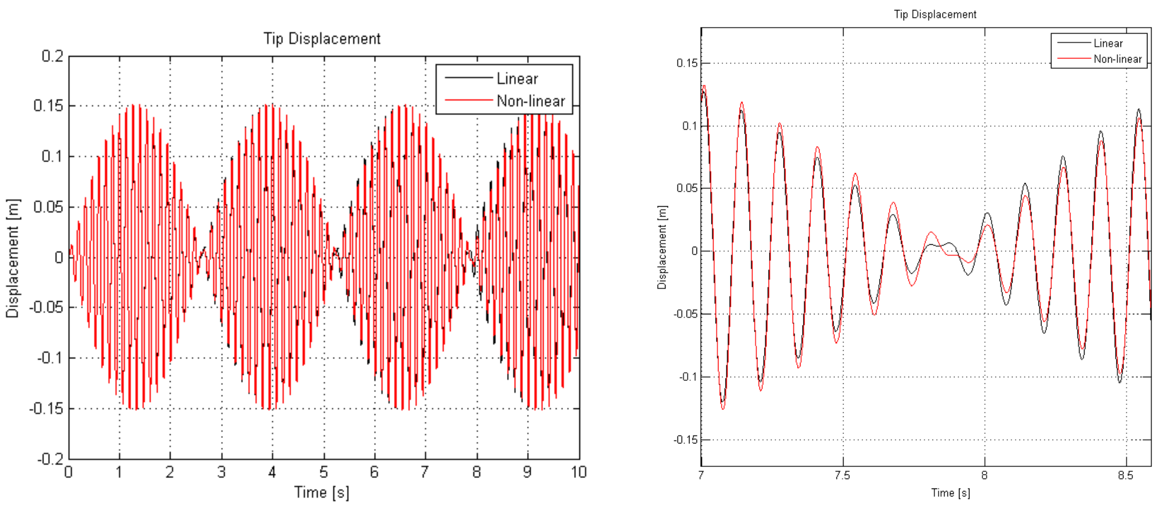

Figure 10. Time history of Multi-mass displacement under the influence of a harmonic load $\boldsymbol{F = 200sin(0.9\omega_1 t)}$ applied at the tip – Comparative analysis between linear & nonlinear models (Left - Zoom).

In order to corroborate the previous result, we develop a new load condition ($\boldsymbol{F = 250sin(0.9\omega_1 t)}$), where we try to observe the same behaviour showed in Figure 11.

Figure 11 presents an increase in the previous observed behaviour, where the appearance of peak in the linear model is followed by a peak slightly lower in the nonlinear model, this effect being seen with greater intensity in the final seconds of simulation. From the data presented in both cases (Fig. 10 & 11), we see a decrease in the threshold frequency where this effect starts. It begins at frequencies 5% lower ($\boldsymbol{\omega = 0.9\omega_1}$) than the resonance regime previously studied (Fig.8, $\boldsymbol{\omega = 0.9\omega_1}$), indicating that the variation of magnitude - for this model - affects the output response.

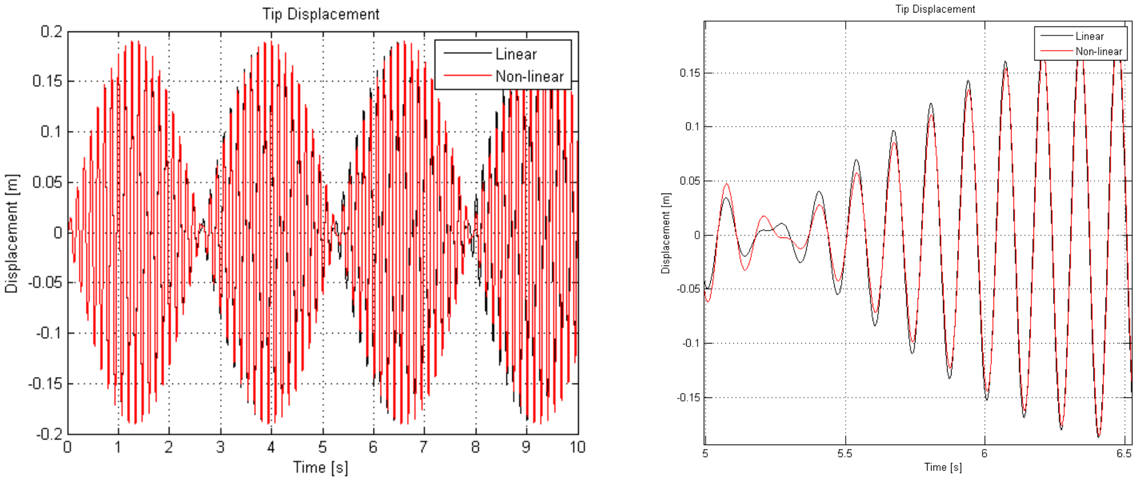

Figure 11. Time history of Multi-mass displacement under the influence of a harmonic load $\boldsymbol{F = 250 sin(0.9\omega_1 t)}$ applied at the tip – Comparative analysis between linear & nonlinear models (Left - Zoom).

In addition, the displacement curves for a hypothetical top amplitude condition ($F_0 = 500N$) are shown in Fig. 12. There we observe the appearance of subtle differences between the linear and nonlinear for a frequency value close to 80%, different from those observed in previous cases, where this behavior appeared at frequencies close to 95% (Fig.9) & 90% (Fig.10-11). This behavior validates the hypothesis previously assumed: an increase in the amplitude load leads to an earlier threshold frequency, the frequency value where we start to observe the difference response between the models.

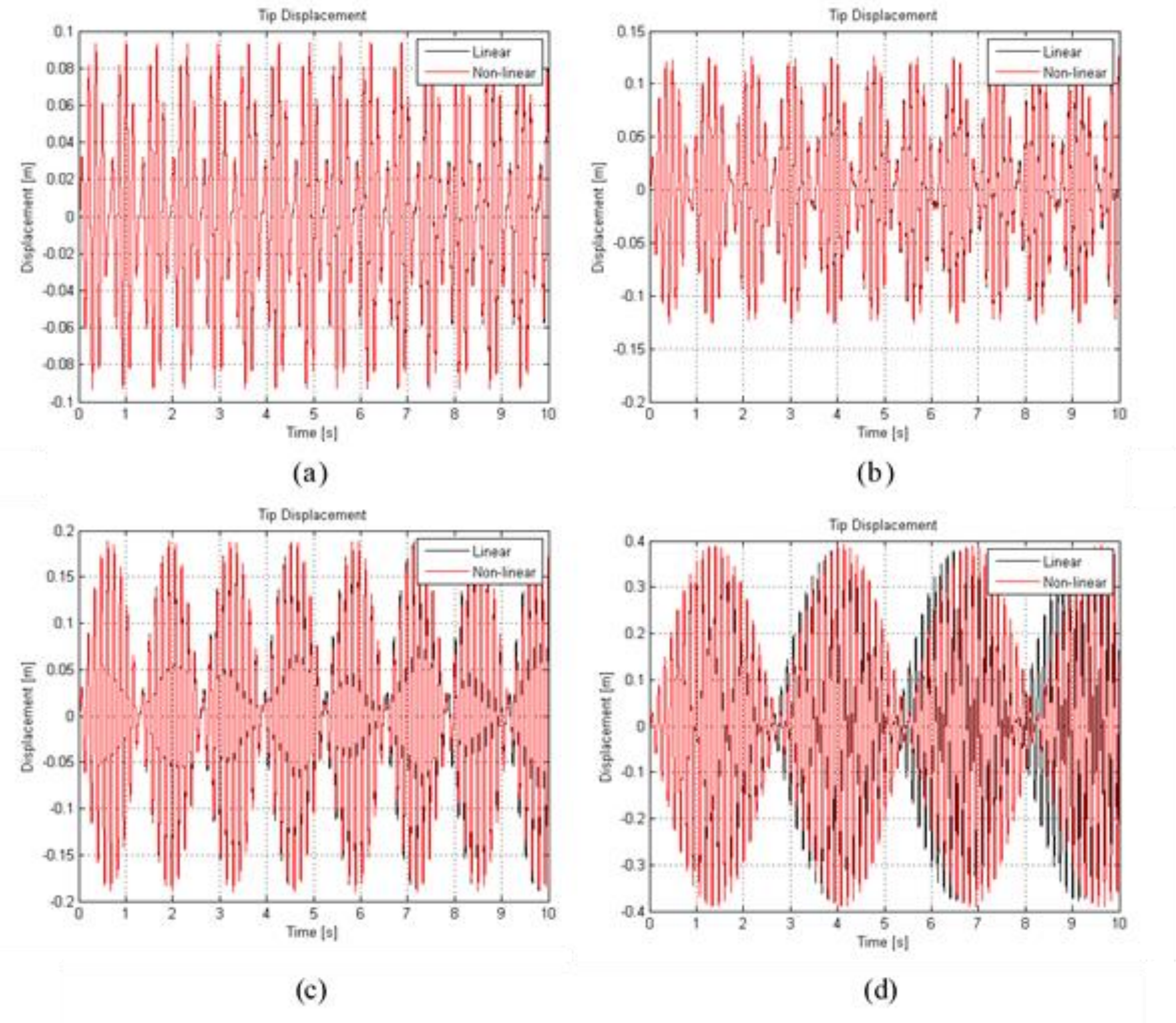

Figure 12. Time history of Multi-mass displacement for a hypothetical load with variable frequency – Comparative analysis between linear & nonlinear models; where: (a) $\boldsymbol{\omega} = \mathbf{0.80\omega_1}$; (b) $\boldsymbol{\omega} = \mathbf{0.85\omega_1}$; (c) $\boldsymbol{\omega} = \mathbf{0.90\omega_1}$ & (d) $\boldsymbol{\omega} = \mathbf{0.95\omega_1}$.

Finally, we apply a harmonic load, whose magnitude decays with time according to an exponential function $F = 100\sin(0.95\omega_1 t)\,e^{-t}$- simulating a satellite control situation (Fig.13). From Fig.13, we can observe that even for frequencies close to the resonance regime, the response of both models - linear and nonlinear - show a maximum response amplitude of 0.043 m.

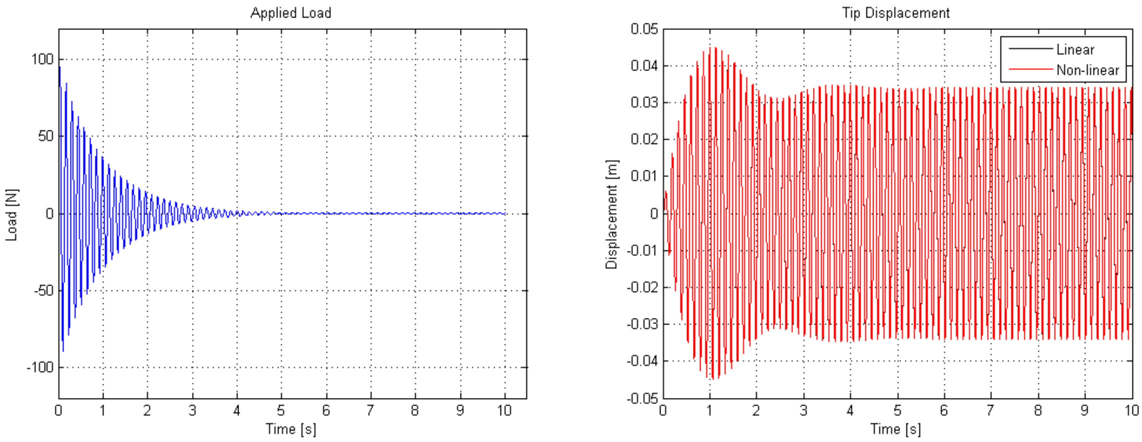

Figure 13. Time history of Multi-mass displacement for a dissipative load condition – Comparative analysis between linear & nonlinear models; (Left) is the applied load and (Right) is the Displacement response.

For the dissipative load condition, it should be noted that unlike the one observed for the harmonic loading response, see Fig. 9, the behavior of both models is identical, leading to the assumption that time-dissipative loading, act as controllers of the system's response, limiting or attenuating the model final response.

1.4 Conclusions

From Belvin et al. (2016), Fetchko et al. (2004), Tupper et al. (2001) e Straubel et al. (2011), we can see the challenges and limitations of current flight-heritage booms, where technological advances in spacecraft appendages, for instance, solar sails, are limited by the old-fashion structural boom designs. This leads us to the need to develop models that can quantify and predict the structural behaviors, especially with respect to lightweight and flexible structures. In this context, we had perform a brief review about lightweight and flexible structures and the development of a multi-mass structure for a comparative study between the dynamic response of linear and nonlinear models. A simplified modeling of the FalconSat-3 boom structure is presented, where it is observed that for flexible structures the consideration of nonlinearity can lead to an unusual behaviour, see Figure 10-12, being evident in simulations where the applied load presents frequencies close to the resonance regime or an increasing in the load amplitude. In conclusion, despite the model small dimensions and the large load value used, this work intended to demonstrate the importance of nonlinear models in the study of flexible structures, where the final response may present slightly different displacement peaks from that provided by linear modeling.

ACKNOWLEDGEMENTS

This research was supported by CAPES (Coordenação de Aperfeiçoamento de Pessoal de Nível Superior. The second author also acknowledges support by CNPq.

REFERENCES

Belvin, W.K., et al., 2016. Advanced Deployable Structural Systems for Small Satellites. *NATO CSO STO Specialist Meeting AVT-257 /RSM-041 on Best Practices for Risk Reduction for Overall Space Systems*, Document Id.20170003919, 12p.

Brasil, R.M.L.R.F., 1990. *Não-Linearidade Geométrica na Dinâmica de Estruturas Aporticadas Planas: Um Tratamento Pelo Método dos Elementos Finitos*. PhD thesis, Universidade de São Paulo (USP).

Clough, R.W. & Penzien, J., 2003. *Dynamics of structures*. Third edition, Computers & Structures, Inc., Berkeley, USA.

Dankanich, J.W., 2015. Small Satellite Propulsion. *Conference on Spacecraft Reconnaissance of Asteroid and Comet Interiors* (AstroRecon), 8-10 Jan. 2015; Tempe, AZ; United States, 20p.

Fetchko, P., et al., 2004. Deployment Optimization of a Boom for FalconSAT-3 Using Elastic Memory Composite Material. *18th Annual AIAA/USU Conference on Small Satellites*, Technical Session VIII: University Programs, 10p.

Liu, Y., Du, H., Liu, L. & Leng, J., 2014. Shape Memory Polymers and Their Composites In Aerospace Applications: A Review. *Smart Materials and Structures*, Volume 23, Number 2, 22p. - doi:10.1088/09641726/23/2/023001.

N/A, 2002. Military Handbook - MIL-HDBK-17-3F: Composite Materials Handbook, Volume 3 - Polymer Matrix Composites Materials Usage, Design, and Analysis. U.S. Department of Defense.

Paz, M., 1985. *Structural Dynamics: Theory and Computation*. Van Nostrand Reinhold Company.

Straubel, M., Block, J., Sinapius, M. & Hühne, C., 2011. Deployable Composite Boom for Various Gossamer Space Structures. *52nd AIAA/ASME/ASCE/AHS/ASC Structures, Structural Dynamics and Materials Conference*. Denver, Colorado, 11p.

Tupper, M., et al., 2001. Developments in Elastic Memory Composite Materials for Spacecraft Deployable Structures. *2001 IEEE Aerospace Conference Proceedings*, IEEE Proceedings, Volume 5, p.2541-2547, doi:10.1109/AERO.2001.931215.

United States Air Force Academy, 2009. *FalconSat Program* [Online]. Available: http://www.usafa.af.mil/About-Us/Fact-Sheets/Display/Article/428292/falconsat-program/ [Accessed 15 August 2017]

Wriggers, P., 2008. *Nonlinear Finite Element Methods*. Springer.